Analytical Methods

PAPER

View Article Online
View Journal | View Issue

Cite this: *Anal. Methods*, 2015, 7, 9918

Green, fast and selective preconcentration of lead ions from various matrices using a novel magnetic sheet-like resin

Mostafa Hossein Beyki,[a] Hassan Alijani[b] and Yousef Fazli*[c]

In this study, an environmentally friendly method has been developed to carry out the fast and selective preconcentration of trace lead ions from water and food samples. For this purpose, a solvent-free route has been employed to prepare Fe_3O_4 and magnetic citric acid–ascorbic acid based resin through mixing the solid reagents. The prepared composite has been characterized with FE-SEM, TEM, FT-IR, VSM, XRD and TGA techniques. The characterization results revealed that the material has a sheet structure and the magnetic nanoparticles are well dispersed on the resin matrix. It was found that the adsorption was very fast as equilibrium was obtained within one min. The selectivity of the sorbent was examined by comparing the behavior of the sorbent for the adsorption of divalent copper, lead, cadmium, cobalt, and zinc from aqueous solutions; the relative selectivity factor (α_r) of Pb^{2+} with respect to the aforementioned cations was 2.45, 3.61, 4.1, and 4.62, respectively. The adsorbed lead ions were stripped from the sorbent using 5 mL of 2 mol L^{-1} hydrochloric acid. The adsorption data was measured at room temperature and yielded a monolayer capacity of 1000 mg g^{-1}. The limit of detection (LOD) and the relative standard deviation were 0.32 μg L^{-1} and 2.85% (n = 6, concentration = 0.1 mg L^{-1}), respectively. Thermodynamic studies reveal that the lead adsorption was spontaneous, which follow an endothermic path with an increase in entropy.

Received 14th September 2015
Accepted 18th October 2015

DOI: 10.1039/c5ay02449h

www.rsc.org/methods

Introduction

The release of various types of waste, such as organic materials, heavy metals, radioactive wastes and gaseous compounds, into water resources and air is a direct effect of the fast development of industrial activity. Most of these hazardous compounds, especially heavy metals, are toxic and non-biodegradable, which have posed a serious threat to ecological systems and public health.[1–5] Among the heavy metals, lead is a highly toxic compound because excessive exposure of it can cause severe damage to the brain, nervous system and may cause neonatal death.[6–9] Consequently, the environmental and health issues associated with heavy metal effluents have become a global crisis.[10] To date, an abundance of materials and techniques have been employed to envisage the removal of heavy metal pollutants. However, only some of them may be viable options for the treatment of waste systems. Adsorption is the most widely applied separation method owing to its higher efficiency and low consumption of pure organic solvents. Choosing an appropriate adsorbent is a key point in the aforementioned method, because this factor can affect the selectivity and sensitivity of the method.[11,12]

Recent advancements reveal that nanotechnology can ameliorate or resolve many issues involving environmental remediation and water quality. In fact, the unique properties of nanomaterials provide inimitable routes to dispel the problematic issue of pollutants in highly efficient and cost-effective approaches.[13,14] Due to the significance of nanomaterials, various sorbents have been proposed such as carbon nanotubes,[15–18] nanoalumina,[19] resin,[20,21] nanoclays,[22] biosorbents,[23,24] graphene,[25] polymeric adsorbent,[26–29] and magnetic nanoparticles.[30,31] Among nanostructured compounds, magnetic nanocomposites are very popular advanced materials that can be guided magnetically and recovered from a solution, and hence are becoming the focus of multidisciplinary studies. Magnetic materials possess unique catalytic, adsorption, optical, and electronic properties, which make them highly desirable for biomedicine, homogeneous catalysis, wastewater processing and many other technological fields.[32–35] There are a wide variety of techniques for producing nanoparticles, especially magnetic compounds, which fall into the three main categories: (i) vapor condensation, (ii) chemical

[a]School of Chemistry, University College of Science, University of Tehran, P.O. Box 14155-6455, Tehran, Iran
[b]Department of Chemistry, Amirkabir University of Technology (Tehran Polytechnic), P.O. Box 15875-4413, Tehran, Iran
[c]Department of Chemistry, Faculty of Science, Islamic Azad University, Arak Branch, Arak, Iran. E-mail: yousef.fazli@gmail.com; y-fazli@iau-arak.ac.ir; Fax: +98 86 33670017; Tel: +98 86 33670017

synthesis and (iii) biological methods.[36–38] These methods are useful for the synthesis of nanomaterials but, they have some disadvantages such as the employment of expensive equipment, requirement of high temperatures or pressures, presence of organic templates and production of harmful gases and polluted wastes from solvents. These drawbacks not only increase the cost, but also result in safety and environmental concerns. Therefore, the development of new, convenient and large-scale synthesis methods to overcome these drawbacks is still a major challenge. Recently, solid-state solvent-free processing has been successfully developed for the synthesis and functionalization of nanomaterials.[39–44] The aforementioned technique can be considered as an efficient and renewable route to prepare and modify nanomaterials. However, in view of environmental remediation, some of the reports in the literature do not match completely with green chemistry's tenet because they use or generate substances that possess toxicity to human health and the environment.[45] In other words, the selection of initial reactants that show compatibility with the environment and human health are more desirable in green chemistry.[46–48]

Based on the reported cases, we have prepared magnetic Fe_3O_4 through a solvent-free route using one iron source, which makes the procedure more economical. Then, a citric acid–ascorbic acid-based resin and its magnetic composite were also synthesized by the thermal reaction of solid raw materials. The procedures are free from harmful gases and do not produce any waste. It is known that the aforementioned substances have natural sources and are dominantly employed as flavoring and preservatives in candy, food and beverages, and as a result they possess little toxicity to ecological systems and human health and can be considered as a green material for lead preconcentration. Effective parameters for lead adsorption have been optimized as well as the isotherm and thermodynamic behaviors have been also evaluated. Finally, the adsorbent was applied for trace lead preconcentration from water and food samples.

Experimental

Materials

Ascorbic acid, citric acid, $FeCl_2 \cdot 4H_2O$, and NaOH were supplied from Merck (Darmstadt, Germany) and applied to prepare a magnetic resin. Standard solutions of heavy metal ions (1000 mg L^{-1}) were prepared by dissolving the nitrate salt in a minimum amount of HNO_3 and then diluted to the appropriate volume using distilled water. pH adjustments were performed using 0.1 mol L^{-1} HCl and NH_3 solutions.

Instruments

The prepared particles were characterized by powder X-ray diffraction analysis using a Phillips powder diffractometer, X′ Pert MPD with Cu-Kα ($\lambda = 1.540589$ Å) radiation in the 2θ range of 2°–100°. FE-SEM and TEM analysis were carried out using HITACHI S 4160 and Zeiss-EM10C instruments. Fourier transform infrared spectra (FT-IR) were obtained using an Equinox 55 Bruker spectrometer with the ATR method over a wavelength range of 400–4000 cm^{-1}. TGA results and magnetization measurements were recorded using a TA-Q-50 and vibration sample magnetometer (VSM) (Lake Shore Model 7400, Japan). A digital pH-meter (model 692, metrohm, Herisau, Switzerland) was used for pH adjustments. A Varian model AA-400 flame atomic absorption (FAAS) spectrometer (Varian Australia Pty Ltd, Musgrave) equipped with a deuterium lamp background and hollow cathode lamp was used for the determination of the metal ions.

Synthesis of Fe_3O_4 and magnetic resin

To prepare Fe_3O_4 nanoparticles, 2.0 g of finely ground $FeCl_2 \cdot 4H_2O$ was mixed with 1.0 g of NaOH for 5 min. Then, the gray particles were dried at 80 °C for 1 h. The resin nanosheet and magnetic nanocomposite were prepared by mixing 1.0 g of ascorbic acid and 0.5 g of citric acid together with 0.5 g of the prepared Fe_3O_4 and heated at 150 °C for 4 h followed by heating at 180 °C for 1 h. After cooling to room temperature, the material was ground and stored for the subsequent investigation. The final yield of the resin was 0.85 g, which is lower than the sum of the initial reagents (1.5 g of citric and ascorbic acid). This situation was attributed to the release of H_2O from the structure of reactants as a result of esterification reaction.

Adsorption experiments

Lead adsorption experiments were performed using a batch method. For this purpose, different amounts of lead ions (0.05–50 mg L^{-1}) were placed in 50 mL volumetric flasks. The pH of the solutions was adjusted to 5–6 and 10 mg of the sorbent was added to each flask. After shaking for one minute, the solid mass was collected and the concentration of ions in the supernatant or in 5 mL of HCl (2.0 mol L^{-1}) as an eluent was determined by FAAS.

Preparation of real samples

500 mL of sea- and well-water samples was adjusted to pH 2.0 using nitric acid after collection, to prevent the adsorption of metal ions on the flask walls and filtered through filter paper to remove any suspended particles and analyzed using the described method. To prepare food and herbal samples, 2.0 g of lettuce, 1.0 g of fish, and 0.5 g of liver were heated separately at 90 °C for 1 h until a constant weight was obtained. After cooling, 10 mL of 65% nitric acid was added, the samples were heated for 45 min and then boiled for at least 10 min until the evolution of brown fumes ceased; 10 mL of 30% hydrogen peroxide was then added. The digestion flask was heated slightly until the sample solutions became clear. The samples were cooled to room temperature, filtered using filter paper, and made up to volume in a 100 mL flask. For determination of lead ions, pH of the samples was adjusted and analyzed using the described procedure. In addition, the accuracy of the method was evaluated by spiking different amounts of lead ions in 50 mL of the sample volume.

Results and discussion

Characterization of the materials

XRD analysis. XRD analysis was used to verify the crystallinity of Fe_3O_4 nanoparticles, resin and magnetic composite. The pattern of Fe_3O_4 (Fig. 1a) showed scattering at $2\theta = 30.12°$, 35.5°, 43.22°, 53.52°, 57.21° and 62.94°, which can be indexed to the (220), (311), (400), (422), (511), and (440) planes of a cubic cell. The results reveal that the nanoparticles have a well-crystalline structure. The preparation of Fe_3O_4 nanoparticles was based on the precipitation–air oxidation of Fe^{2+} ions.[49] In the first step, Fe^{2+} precipitates as $Fe(OH)_2$ and owing to its exposure to air, $Fe(OH)_2$ was partially oxidized to Fe(OOH), which in the subsequent step condensed and formed Fe_3O_4. The reactions during the synthesis process are as follows:

$$FeCl_2{\cdot}4H_2O_{(s)} + 2NaOH_{(s)} \rightarrow Fe(OH)_2 + 2NaCl_{(s)} + 4H_2O \quad (1)$$

$$4Fe(OH)_2 + O_2 \rightarrow 4Fe(OOH) + 2H_2O \quad (2)$$

$$2Fe(OH)_2 + Fe(OOH) + OH^- \rightarrow Fe_3O_{4(s)} + 3H_2O \quad (3)$$

The XRD pattern of the citric acid–ascorbic resin (Fig. 1a) shows a main broad scattering beginning from 10° to 50° with a maximum height at 17.4°. The XRD pattern of magnetic nanocomposite was dominant with the main peak of resin and confirms that the incorporation of nanoparticles within the resin exerts a low effect on its crystallization. However, the characteristic peak of Fe_3O_4 was also observed as a very small peak, which confirmed the formation of the Fe_3O_4@resin nanocomposite. It is obvious that the crystalline behavior of Fe_3O_4 is considerably affected by the growth of the resin on its surface. Moreover, this means that the deposition of resin on the surface of the nanoparticles hinders the crystallinity of Fe_3O_4. As a result, the lower intensity of Fe_3O_4 peaks was due to the small particle size of the nanoparticle phase, which was below the limit of detection of XRD. Moreover, the dilution effect or presence of large amounts of the resin on the nanoparticle surface causes masking of the diffraction peaks of the Fe_3O_4 nanoparticles.

FT-IR spectra. The FT-IR spectra of Fe_3O_4 and the nanocomposite are shown in Fig. 1b. In the Fe_3O_4 structure, Fe–O stretching appears at 400–600 cm^{-1}, which was ascribed to the stretching vibration of octahedral and tetrahedral complexes.[50] However, the adsorption peaks of the nanoparticles at the aforementioned positions mainly depend on the vibration of the octahedral group. In addition, the peaks with high intensity are due to the increased molecular vibration as a result of the high crystallinity of the nanoparticles. The characteristic OH bending vibration and stretching vibration of the residual hydroxyl groups appear at 3000–3500 cm^{-1}. The appearance of the hydroxyl vibration was attributed to the surface functional groups and water molecules in the Fe_3O_4 structure. Moreover, the H–O–H bending vibration with low intensity was found at about 1000–1600 cm^{-1} as a result of H_2O molecules. The spectrum of the magnetic resin appears to have new absorbance

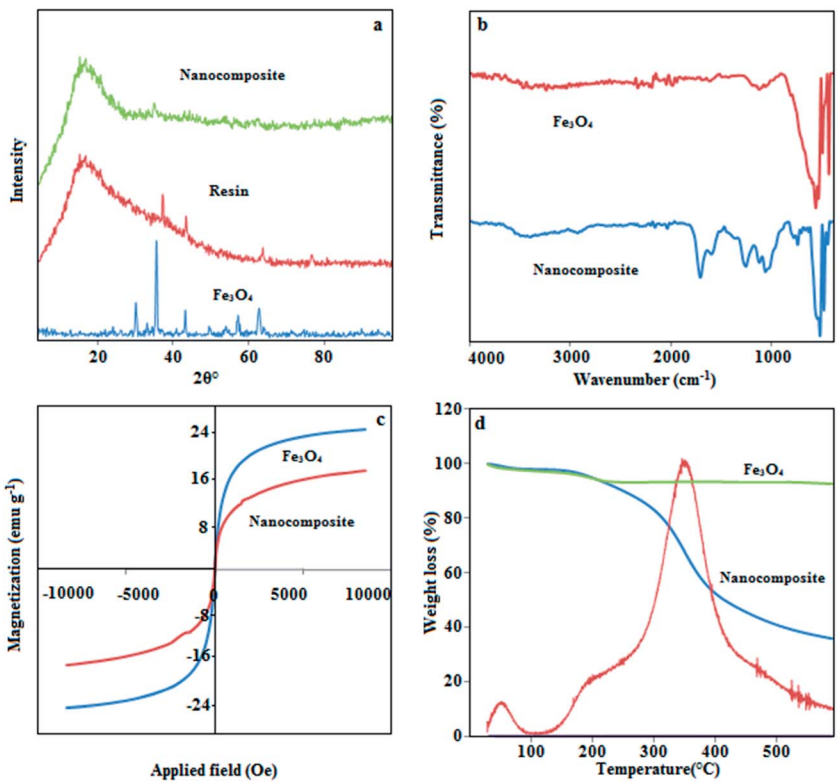

Fig. 1 The XRD pattern (a), FT-IR spectra (b), VSM graph (c) and TGA profile (d) of as-synthesised Fe_3O_4 and the nanocomposite.

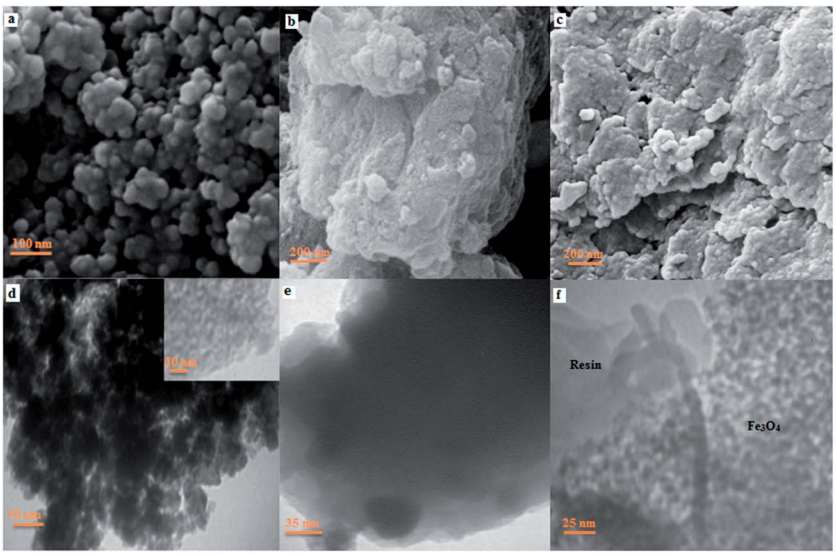

Fig. 2 The FE-SEM images of Fe_3O_4 (a), resin (b), and magnetic nanocomposite (d). The TEM images of Fe_3O_4 (d), resin (e), and the magnetic nanocomposite (f).

peaks at 3500, 2960, 1725, 1000–1500 and 523 cm^{-1}, which correspond to the characteristic functional groups of the pristine resin. The peak in the region around 3500 cm^{-1} is assigned to the stretching vibration of free –OH groups. Furthermore, the peaks at 2960 and 1725 cm^{-1} correspond to C–H stretching and C=O vibrations, respectively. The vibration of C=C, symmetric stretching of C–OH and bending vibration of CH_2 groups appeared at 1000–1600 cm^{-1}.[51] The peaks at 800–1000 cm^{-1} belong to C–H out-of-plane bending.[52] It is obvious that the peaks of the magnetic nanoparticles were also observable in the 400–600 cm^{-1} region of the spectrum of the magnetic resin nanocomposite and confirm that the nanoparticles are present in the resin matrix.

Magnetic characteristics. The magnetic hysteresis loops for the prepared materials are shown in Fig. 1c. The magnetization of the materials exhibits a clear hysteresis behavior. The value of saturation magnetization (M_s) for the as-synthesized Fe_3O_4 was 24 emu g^{-1}, which was lower than that of bulk Fe_3O_4 (89–95 emu g^{-1}). It is known that disorder in the magnetic moment orientation of the particles causes dispersion in the exchange constant and as a result suppresses the saturation magnetization of the nanoparticles. In other words, magnetic moments have a ferrimagnetic alignment between tetrahedral and octahedral sites, as a result an increase in the occupation ratio of Fe^{3+} ions at the octahedral sites decreases the net magnetic moment.[53] In addition, the saturation magnetization usually decreases with decrease in particle size, owing to spin canting occurring in the disordered surface layer. From the magnetic coefficients, the M_s value for magnetic resin (16 emu g^{-1}) was also observed to be less than those obtained for pure nanoparticles. This was attributed to the lower volume fraction of the magnetic nanoparticles relative to the total volume of the nanocomposite[54] as well as disaffiliation of the coated layer on the total magnetization. The M_r value for the nanoparticles and the nanocomposite was 0.008 and 0.003, respectively, which indicate that they possess superparamagnetic properties.[55] This

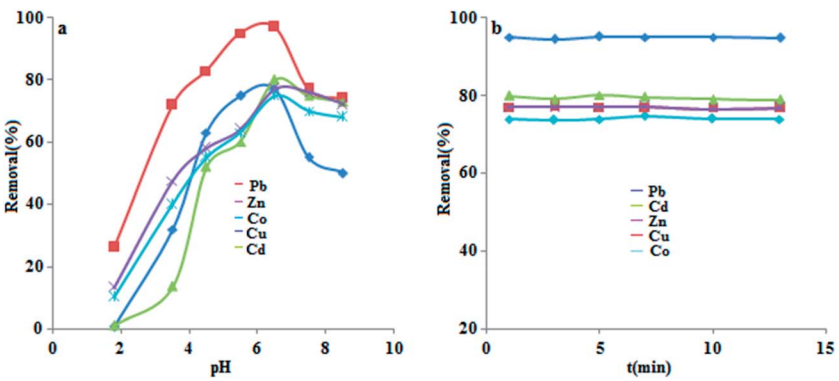

Fig. 3 The effect of pH (a) and time (b) on heavy metal adsorption using the magnetic resin. Conditions: volume; 50 mL, adsorbent; 10 mg, and metal concentration; 2 mg L^{-1}.

Table 1 Data for lead adsorption based on the Langmuir and Freundlich adsorption models using the Fe_3O_4@resin. Conditions: volume; 50 mL, adsorbent; 10 mg, pH; 6–7, time; 1 min, and concentration; 10–50 and 100–1000 mg L^{-1}

Langmuir					Freundlich			
C_0 (mg L^{-1})	R^2	Q_m (mg g^{-1})	b	χ^2	R^2	K_f	n	χ^2
10–50	0.950	1000	3.5×10^{-5}	3.6	0.954	34.46	1.30	4.4
100–1000	0.930	1025	2.3×10^{-2}	42.19	0.976	225.80	4.34	11.51

can be attributed to the fact that the particle size is so small that each particle is a single magnetic domain.[56]

TGA analysis. Thermal stability of the material is important, especially when it is considered to be used at elevated temperatures. Study of the thermal stability of the prepared nanocomposite can be carried out using thermogravimetric analysis (TGA). The TGA curves of the nanoparticles and nanocomposite are shown in Fig. 1d. The weight loss for the nanoparticles in the range of 20–600 °C was quite small (5%) because of the removal of volatile moisture. The nanocomposite undergoes three stages of weight loss, one at 20–100 °C with a 3% loss, another at around 200 °C with a 7% loss in the resin mass, and at more extreme temperatures, a third main weight loss with 49.5% loss appears. As a result, the nanocomposite undergoes a weight loss of about 60%. In other words, the magnetic Fe_3O_4 residual material content is approximately 40 wt%. The first weight loss was due to the volatile low-molecular-weight compounds, which are generated as a result of fragmentation reactions in the synthesis step. The second weight loss may be attributed to the re-crystallization and crosslinking reactions of the resin chains. Moreover, the third main weight loss can be assigned to the decomposition and degradation of the resin backbone, which is accompanied by the release of volatile gasses such as carbon dioxide. The DTA graph of the nanoparticles exhibits no significant peaks beside the one for the nanocomposite and shows one strong peak at around 340 °C, which was initiated from 250 °C as the tolerance threshold and smoothly continued to 600 °C.

SEM and TEM analysis. The FE-SEM image of Fe_3O_4 (Fig. 2a) exhibits spherical crystals in discrete bundles. Further analysis using the TEM image (Fig. 2d) shows the high density of the nanoparticles composed of fine particles with diameters of less than 5 nm. The formation of spherical shapes was attributed to isotopic nucleation at the interface between the Fe_3O_4 magnetic nanoparticles[57] because the driving force for Ostwald ripening minimizes the surface free energy by reducing the total surface

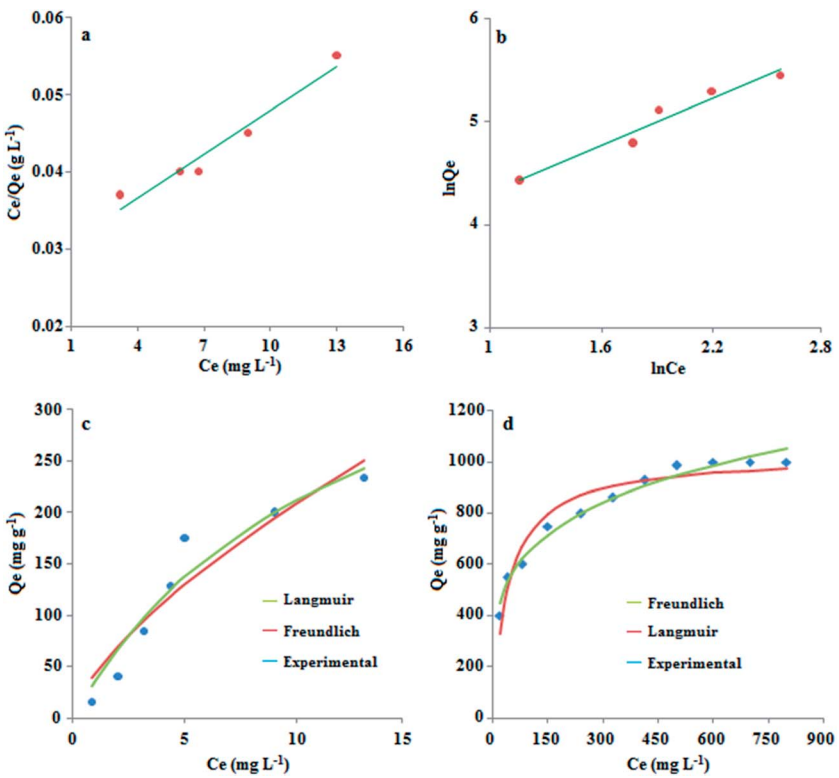

Fig. 4 A typical linear Langmuir (a) and Freundlich (b) isotherm model. Conditions: volume; 50 mL, time; 1 min, adsorbent; 10 mg and concentration; 10–50 mg L^{-1}. The non-linear isotherms at 10–50 mg L^{-1} (c) and 100–1000 mg L^{-1} (d).

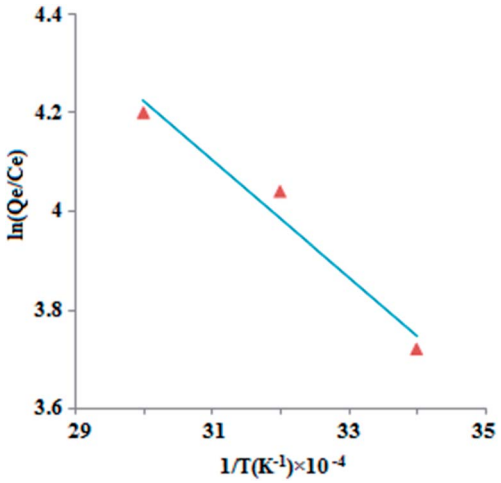

Fig. 5 The relationship curve between ln K_c and 1/T. Conditions: volume; 50 mL, time; 1 min, adsorbent; 10 mg, and concentration; 4 mg L^{-1}.

Table 2 Thermodynamic parameters for the adsorption of lead ions onto the magnetic resin as a function of temperature. Conditions: volume; 50 mL, adsorbent; 10 mg, pH; 6–7, time; 1 min, and concentration; 4 mg L^{-1}

Temperature (K)	ΔG (kJ mol^{-1})	ΔS (J K^{-1} mol^{-1})	ΔH (kJ mol^{-1})
293	−9.06	+65.01	+9.97
313	−10.05		
333	−11.62		

area/volume. This situation induces an equivalent growth rate along the different directions of nucleation and results in the formation of sphere-like morphology.[58] Fig. 2b shows the FE-SEM image of the as-prepared resin. It indicates that the resin exhibits a stacked sheet-like and thin lamellar structure on the macro-level. Moreover, the TEM image (Fig. 2e) shows that the obtained sheets are very slim because the thickness of the micrometer lamellar structure is less than 5 nm. The structures of citric acid and ascorbic acid contain several potential active sites (hydroxyl and carboxylic acid groups), which can participate in a condensation reaction. The reaction can proceed in various directions through esterification between the acid–hydroxyl functional groups. The direct result of this situation is the sheet-like structure. Moreover, lamellar layers can be regarded as the combined structure of oxygen-containing functional groups, such as C–O, C═O, and –OH, supported on the surface of the resin sheet. According to the FE-SEM and TEM results (Fig. 2c and f), the dispersion of magnetic nanoparticles was obvious in the composite structure. However, it was observed that the nanoparticles dispersion was not homogeneous in the resin matrix. It is known that there is a OH rich surface in the Fe_3O_4 structure,[59] which can react with acidic groups, and as a result the magnetite nanoparticles can be attached to the resin by a chemical bond. This phenomenon can be explained by the replacement of Fe–OH groups on the surface of the Fe_3O_4 particles by Fe–O–C bonds.

The effect of temperature on resin stability. It seems that the synthesis temperature has a main effect on the stability of the product. Some portion (0.1 g) of the product obtained at 150 °C was dispersed in distilled water and then collected by centrifugation. It was observed that the supernatant had a yellow color owing to the dissolution of the resin. Moreover, the weight of the resin decreased by about 10%. The same experiment was performed for the product obtained at 180 °C and no loss was observed for the product. This can be explained by the fact that at lower temperatures only the first type of hydroxyl groups reacts with the acidic groups. Higher temperatures induce the reaction of second type hydroxyl groups and promote linkages between the functional groups, which lead to the formation of sheets with a hyper cross-linked structure.

Optimizing heavy metal adsorption variants

The effect of pH and time on metal adsorption. To evaluate the metal adsorption properties of the nanocomposite, the basic centers of the magnetic resin available have been used for the adsorption of divalent lead, copper, cadmium, cobalt and zinc from an aqueous solution. The influence of solution pH on metal adsorption was examined over the pH range of 2.0–10.0.

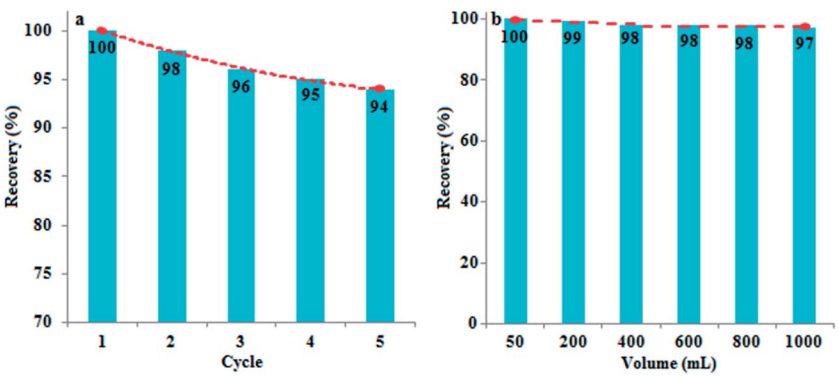

Fig. 6 Number of regeneration cycles of the magnetic resin (a) and the effect of the sample volume on lead recovery (b). Conditions: adsorbent; 10 mg, metal concentration; 0.1 mg L^{-1}, shacking time; 1 min and eluent 5 mL of 2 mol L^{-1} HCl solution.

Table 3 The effect of interfering ions on lead recovery. Conditions: volume; 50 mL, adsorbent; 10 mg, pH; 6–7, time; 1 min, and lead concentration; 0.1 mg L^{-1}

Ion	Ratio ion/Pb	Recovery
Mn^{2+}	600	97 ± 1
Zn^{2+}	500	95 ± 2
Cd^{2+}	650	98 ± 1
Cr^{3+}	500	95 ± 1
Ni^{2+}	500	94 ± 2
Cu^{2+}	250	94 ± 2
Co^{2+}	500	100 ± 1
Na^{+}	5000	92 ± 1
K^{+}	7000	98 ± 1
Mg^{2+}	1000	92 ± 1
Ca^{2+}	1000	100 ± 1
Cl^{-}	7000	100 ± 2
HPO_4^{2-}	8000	93 ± 1

About 10 mg of the adsorbent was suspended in 50 mL of the metal solutions (2.0 mg L^{-1}) maintained at several pH values. These samples were shaken for 10 min, then the sorbent was separated and removal percentage was calculated using the following equation:

$$R\% = (C_0 - C_e) \times 100/C_0 \quad (4)$$

where C_0 and C_e are the initial and equilibrium concentrations (mg L^{-1}) of the metal ions in the solution, respectively. The results shown in Fig. 3a show that the maximum removal of the heavy metals onto the adsorbent was obtained at a pH of more than five. The dependence of heavy metal sorption on pH is related to the metal species in the solution. By changing the pH of the solution, the ion was predicted to exist predominantly as monomeric species and multi-nuclear oligomeric hydroxide complexes; hence, the adsorption of heavy metal ions onto the nanocomposite can be described as a chemical coordination and electrostatic process. The increase in the ion's removal with pH increases was on the basis of the fact that there is a decrease in the positive surface charge following a decrease in the competition between H_3O^+ and the metal ions. Moreover, at a higher pH, the positive species of the ions may be effectively adsorbed with the negative charge of the sorbent; hence, the removal efficiency of the ions increases at a high pH value. A greater increase in pH value causes the precipitation of the ions and decreases the metal adsorption efficiency. From the results, it can be seen that the maximum removal of lead ions of 95–98% is in the pH range of 6–7. However, it can be observed that the maximum removal of other ions was 80% under the same conditions.

In this study, the extraction time was varied from 1 to 13 minute. A 50 mL solution containing 10 mg of the adsorbents and 2.0 mg L^{-1} of the metal ions at pH 6–7 was used in this experiment. According to the results (Fig. 3b), the removal efficiency in the first minute was 95%, 77%, 80%, 76% and 75% for Pb^{2+}, Cu^{2+}, Cd^{2+}, Zn^{2+} and Co^{2+}, respectively. Upon further interaction time, the removal efficiency was not changed as a result the equilibrium time of one minute was selected for subsequent investigations. Such a fast adsorption rate can be attributed to the external surface adsorption and the absence of internal diffusion resistance, which were accompanied with a microporous adsorption process. This behavior indicates that the chelating sites at the surface of the adsorbents are easily accessible by the metal ions. According to the results of contact time and solution pH, it can be concluded that the adsorbent has more efficiency for lead adsorption relative to the other ions; hence, the adsorbent was employed as a solid-phase extraction system for lead preconcentration. Moreover, the lead adsorption characteristics have been studied in more detail.

Adsorption capacity. The sorption of metal ions is a physical or chemical process at an interface of liquid and solid phases that can be revealed by the adsorption behavior of the target ions at the surface of the adsorbent. Among the adsorption models, Langmuir and Freundlich isotherm equations have been widely used to predict the adsorption capabilities of the metals on solid sorbents. The Langmuir model (eqn (5)) verifies that the sorbent is structurally homogeneous and that all the sorption sites are energetically the same and correspond to a dominant ion exchange mechanism,[60] while the Freundlich isotherm (eqn (6)) shows the adsorption–complexation reactions that take place in the adsorption process.[61]

$$C_e/Q_e = C_e/Q_m + 1/b\ Q_m \quad (5)$$

$$\ln\ Q_e = \ln\ K_f + 1/n\ \ln\ C_e \quad (6)$$

where Q_e is the amount of metal ions adsorbed per unit mass of the sorbent (mg g^{-1}) and C_e is the amount of metal ions in the liquid phase at equilibrium (mg L^{-1}). The Q_m is the maximum adsorption capacity and b is the Langmuir coefficient.[62] The results of the adsorption models at two concentration ranges (10–50 mg L^{-1} and 100–1000 mg L^{-1}) are depicted in Table 1. It can be seen that in the low concentration range, the Langmuir model shows a good linearity for lead ions. However, the linearity of the Freundlich model was also high; hence, it may be concluded that the adsorption process can also be explained

Table 4 The results for the analysis of lead ions from water and food samples. Conditions: volume; 50 mL, adsorbent; 10 mg, pH; 6–7, and time; 1 min

Sample	Added (μg L^{-1})	Found (μg L^{-1})	Recovery (%)
River water	0	—	—
	50	51	102 ± 1
Sea water	0	10	—
	50	58	96 ± 1
Liver	0	6	—
	50	55	98 ± 2
Mushroom	0	7	—
	50	55.5	97 ± 2
Fish	0	6.8	—
	50	55	96.4 ± 1
Lettuce	0	4.4	—
	50	52.4	96 ± 2

reasonably by the Freundlich model. The accuracy of the isotherm models was further evaluated by a chi-square test (χ^2). This error function is given by eqn (7), where Q_{exp} and Q_c are the experimental data and that calculated from the non-linear model.[63]

$$\chi^2 = \sum \frac{(Q_{exp} - Q_c)^2}{Q_c} \quad (7)$$

Based on the results given in Table 1 and Fig. 4a–c, the Langmuir model has a lower χ^2 value and reveals that this model can better describe the adsorption behavior of lead ions by the adsorbent. Further studies at high concentrations (Fig. 4d) show that the adsorption behavior has been reversed because the Freundlich model fits well with the experimental values. These results indicate that the adsorption process follows a complex mechanism as lead sorption occurs along with a physicochemical sorption process.

Thermodynamic studies. The adsorption capacities of lead with an initial concentration of 4 mg L^{-1} and an adsorbent dosage of 10 mg were 17.82, 18.36 and 18.58 mg g^{-1} at 293, 313 and 333 K, respectively. These results indicate that lead adsorption onto the nanocomposite is favorable at higher temperatures. The thermodynamic parameters for the adsorption process, such as ΔH (kJ mol^{-1}), ΔS (J K^{-1} mol^{-1}) and ΔG (kJ mol^{-1}), were evaluated using the following equations:

$$\Delta G = -RT \ln(Q_e/C_e) \quad (8)$$

$$\Delta G = \Delta H - T\Delta S \quad (9)$$

$$\ln(Q_e/C_e) = \Delta S/R - \Delta H/RT \quad (10)$$

where R and T are the gas constant (8.314×10^{-3} kJ K^{-1} mol^{-1}) and absolute temperature (K), respectively. The plot of $\ln(Q_e/C_e)$ *versus* $1/T$ was linear (Fig. 5) with the slope and the intercept giving the values of ΔH and ΔS, respectively.[64] The results in Table 2 indicate that the lead–magnetic resin interactions were accompanied by a decrease in the Gibbs energy, which makes the interactions spontaneous and suggests that the process is feasible at higher temperatures. The endothermic enthalpy change, ΔH, for lead adsorption in 293 K was calculated to be +9.97 kJ mol^{-1}. The entropy increased for lead adsorption as the value of ΔS for this interaction was calculated to be +65.01 J K^{-1} mol^{-1} as a result the adsorption process was entropy stabilized.

Selectivity of the sorbent. Competitive enrichment of the lead ions with respect to zinc, copper, cobalt and cadmium from 50 mL of a binary solution containing 2.0 mg L^{-1} of lead and each ion was also investigated and the relevant parameters were calculated by the following equations:

$$D = 1000Q/C_e \quad (11)$$

$$\alpha_{Cu}/\alpha_M = D_{Cu}/D_M \quad (12)$$

where D is the distribution ratio (mL g^{-1}), α_{Cu}/α_M is the selectivity coefficient, and D_{Cu} and D_M represent the distribution ratios of Pb^{2+} and M^{n+}, respectively.[65] The values of distribution factor for Pb^{2+} with respect to Cd^{2+}, Co^{2+}, Cu^{2+} and Zn^{2+} were 3.6, 4.1, 2.45 and 4.62, respectively, which are higher than one, and confirm specificity of the composite for lead ions.

Regeneration of the sorbents. To evaluate the possibility of regeneration of the adsorbent, desorption experiments were also performed. According to the results from the effect of pH, the adsorption was not efficient in an acidic medium; hence, it can be assumed that elution with an acidic solution can be favorable. Thus, HCl solutions at different concentrations (0.1–2.0 mol L^{-1}) were examined as eluents. The results of this study indicated that with a change in the eluent concentration (0.1, 0.5, 1.5 and 2.0), the recovery increased and reached to about 98% using 5 mL of a 2 mol L^{-1} eluent. Moreover, to evaluate the reusability of the magnetic nanocomposite, they were subjected to several loadings with the lead sample solution and subsequent elution. It was found that the recovery was in the range of 94–98% after five cycles of sorption and desorption (Fig. 6a).

The effect of interfering ions. To investigate the effect of co-existing ions on the adsorption of lead ions, 50 mL of the sample solution with a concentration of 0.1 mg L^{-1} with respect to lead ions and a given amount of interfering ions were analyzed according to the adsorption procedure. The results are

Table 5 A comparison of the lead adsorption properties of the prepared material with some previously reported sorbents

Method	PF	LOD (μg L^{-1})	RSD (%)	LDR (μg L^{-1})	Q_e (mg g^{-1})	Time (min)	Ref.
4-Aminoazo-benzene-MWCNT	150	0.28	2.1	0.98–82	46.8	10	9
Nanoporous silica	100	0.45	3.1	3–100	208	3	11
SDS–alumina	292	0.75	1.9	0.02–0.8	6.4	12	12
MWCNT	80	0.6	<5	—	10.3	10	16
PAN-MWCNT	120	0.32	1.7	0.83–15	9.3	50	17
MWCNT	20	8	2.5	—	—	25	18
2-Mercaptobenzo-thiazole resin	20	5	2.4	1–12	—	50	20
Graphene oxide	—	1.4	4	5–100	—	5	25
Ion-imprinted sol–gel	—	0.23	3.7	—	221	20	26
Ion-imprinted polymer	245	0.42	2.1	—	75.4	5	28
Diethylenetriamine–magnetic graphene oxide	167	0.38	1.86	1.35–110	172.41	10	30
Pyridine–magnetic mesoporous silica	200	0.1	2.5	0.9–200	287	5	31
Magnetic resin	200	0.32	2.85	2–120	1000	1	This work

shown in Table 3 and indicate that the preconcentration system has a good tolerance limit for lead preconcentration in the presence of a high level of potential interfering ions.

Analytical characteristics. The calibration curve for lead, based on the optimal conditions, was found to be linear with a correlation coefficient of 0.992 in the range of 2.0–120 μg L^{-1}. The limit of detection and relative standard deviation (RSD) of Pb(II) were 0.32 μg L^{-1} and 2.85%, respectively. To evaluate the potential of the SPE system for lead preconcentration from high volumes, the effect of sample volumes from 50 to 1000 mL containing 5 μg of lead was studied under the optimum conditions using the described method. The results are depicted in Fig. 6b and reveal that the target ions were quantitatively recovered when the sample volume was around 1000 mL, and after elution with 5 mL of the eluent, an enrichment factor of 200 was achieved.

Application of the method. The accuracy of the developed procedure was evaluated by determination of lead in water and acid-digested samples. The results are depicted in Table 4 and indicate that the recovery of the spiked samples was satisfactory (in the range of 96–102%). This result indicates the capability of the system to determine the analyte in real samples with different matrices.

Comparison of the adsorbent performance. The Fe_3O_4@resin nanocomposite has been used for preconcentration of divalent lead ions from aqueous media. The results (Table 5) indicate that the adsorbent possesses two prominent advantages relative to other adsorbents *i.e.*, a fast adsorption time as the equilibrium was obtained in the first minute and an excellent adsorption capacity of 1000 mg g^{-1} was observed for lead ions. The other main characteristics of the method were its good limit of detection, high tolerance limit with regard to interfering ions and good reusability of the adsorbate. Moreover, the prepared nanocomposite is considered to be a green adsorbent, which has been prepared by a simple method using inexpensive precursors.

Conclusions

In summary, we have developed a solvent-free synthesis conditions giving access to magnetic Fe_3O_4 and a magnetic nanoparticles reinforced sheet-like resin. The method as a highly sustainable way exhibits some benefits such as the use of one iron source, the employment of non-toxic organic reagents from natural sources, the avoidance of harmful gases, which is ecologically beneficial, and generates substances that possess low toxicity to human health and the environment. In brief, a simple and convenient procedure has been employed, which saves energy and reduces the cost of the synthesis of the materials. In view of its potential applications, the basic centers of the magnetic resin available were employed for the fast and selective preconcentration of lead ions from water and food samples, and optimum conditions for extraction of the ion were reported in detail. The method has a fast equilibrium time, relatively high tolerance limit for interfering ions, good selectivity, high preconcentration factor (200), and acceptable efficiency for the preconcentration of lead ions from real samples. The retained metal ions can be eluted using HCl solution. Moreover, the adsorbent showed good reusability and adsorption capacity for lead ions. The lead–resin interactions were accompanied by an increase in the ΔS value and an endothermic enthalpy change. Moreover, the kinetics of the interactions as well as isotherm models have been described using a pseudo-second order mechanism and Langmuir model.

Acknowledgements

Support of this study by the research council of Islamic Azad University, Arak Branch is gratefully acknowledged.

References

1 H. Hadjara, B. Hamdi and C. O. Ania, *J. Hazard. Mater.*, 2011, **188**, 304–310.
2 H. Yu and B. Fugetsu, *J. Hazard. Mater.*, 2010, **177**, 138–145.
3 Y. Ren, H. A. Abbood, F. He, H. Peng and K. Huang, *Chem. Eng. J.*, 2013, **226**, 300–311.
4 X. Cheng, X. Huang, X. Wang, B. Zhao, A. Chen and D. Sun, *J. Hazard. Mater.*, 2009, **169**, 958–964.
5 Z. Cheng, Z. Gao, W. Ma, Q. Sun, B. Wang and X. Wang, *Chem. Eng. J.*, 2012, **209**, 451–457.
6 Y. Chen, L. Ding and J. Nie, *Desalin. Water Treat.*, 2012, **44**, 168–173.
7 Y. Li, T. Qiu and X. Xu, *Eur. Polym. J.*, 2013, **49**, 1487–1494.
8 R. E. Green and D. J. Pain, *Food Chem. Toxicol.*, 2012, **50**, 4180–4190.
9 Z. Li and L. Wu, *Int. J. Environ. Anal. Chem.*, 2014, **94**, 291–303.
10 C. L. Warner, W. Chouyyok, K. E. Mackie, D. Neiner, V. Saraf, T. C. Droubay, M. G. Warner and R. S. Shane Addleman, *Langmuir*, 2012, **28**, 3931–3937.
11 M. Behbahani, M. Salarian, M. M. Amini, O. Sadeghi, A. Bagheri and S. Bagheri, *Mod. Methods Food Anal.*, 2013, **6**, 1320–1329.
12 M. Ghaedi, K. Niknam, A. Shokrollahi, E. Niknam, H. R. Rajabi and M. Soylak, *J. Hazard. Mater.*, 2008, **155**, 121–127.
13 A. Kaur and U. Gupta, *J. Mater. Chem.*, 2009, **19**, 8279–8289.
14 J. Liu, Z. Zhao and G. Jiang, *Environ. Sci. Technol.*, 2008, **42**, 6949–6954.
15 M. Soylak and Z. Topalak, *J. Ind. Eng. Chem.*, 2014, **20**, 581–585.
16 M. Tuzen, K. O. Saygi and M. Soylak, *J. Hazard. Mater.*, 2008, **152**, 632–639.
17 S. Z. Mohammadi, D. Afzali and D. Pourtalebi, *Cent. Eur. J. Chem.*, 2010, **3**, 662–668.
18 S. Gollu Ozcan, N. Satiroglu and M. Soylak, *Food Chem. Toxicol.*, 2010, **48**, 2401–2406.
19 M. Medina, J. Tapia, S. Pacheco, M. Espinosa and R. Rodriguez, *J. Non-Cryst. Solids*, 2010, **356**, 383–387.
20 S. Tokalioglu, A. Papak and S. Kartal, *Arabian J. Chem.*, 2013, DOI: 10.1016/j.arabjc.2013.04.017.
21 A. Islam, A. Ahmad and M. A. Laskar, *Clean: Soil, Air, Water*, 2012, **40**, 54–65.

22 R. Rojas, *Appl. Clay Sci.*, 2014, **87**, 254–259.
23 A. Jakóbik-Kolon, A. K. Milewski, K. Mitko and A. Lis, *Sep. Sci. Technol.*, 2014, **49**, 1679–1688.
24 P. K. D. Chathuranga, D. M. R. E. A. Dissanayake, N. Priyantha and S. S. Iqbal, *Biorem. J.*, 2014, **18**, 192–203.
25 B. Zawisza, R. Sitko, E. Malicka and E. Talik, *Anal. Methods*, 2013, **5**, 6425–6430.
26 L. Wang, M. Zhou, Z. Jing and A. Zhong, *Microchim. Acta*, 2009, **165**, 367–372.
27 L. Jin and R. Bai, *Langmuir*, 2002, **18**, 9765–9770.
28 M. Behbahania, A. Bagheri, M. Taghizadeh, M. Salarian, O. Sadeghi, L. Adlnasab and K. Jalali, *Food Chem.*, 2013, **138**, 2050–2056.
29 A. Duran, M. Soylak and S. A. Tuncel, *J. Hazard. Mater.*, 2008, **155**, 114–120.
30 E. Aliyari, M. Alvand and F. Shemirani, *Anal. Methods*, 2015, **7**, 7582–7589.
31 M. Behbahani, A. Ali Akbari, M. M. Amini and A. Bagheri, *Anal. Methods*, 2014, **6**, 8785–8792.
32 W. Cai, J. Yu, C. Anand, A. Vinu and M. Jaroniec, *Chem. Mater.*, 2011, **23**, 1147–1157.
33 D. Dupont, W. Brullot, M. Bloemen, T. Verbiest and K. Binnemans, *ACS Appl. Mater. Interfaces*, 2014, **6**, 4980–4988.
34 M. Baghayeria, E. Nazarzadeh Zare and M. Mansour Lakouraj, *Biosens. Bioelectron.*, 2014, **55**, 259–265.
35 C. Cao, J. Qu, W. Yan, J. Zhu, Z. Wu and W. Song, *Langmuir*, 2012, **28**, 4573–4579.
36 J. Morales, L. M. Apatiga and V. M. Castano, *Rev. Adv. Mater. Sci.*, 2009, **21**, 134–138.
37 S. Chen, *Ind. Eng. Chem. Res.*, 1996, **35**, 4487–4493.
38 D. Bhattacharya and R. K. Gupta, *Crit. Rev. Biotechnol.*, 2005, **25**, 199–204.
39 Q. Wu, X. Wang, G. Qi, Q. Guo, S. Pan, X. Meng, J. Xu, F. Deng, F. Fan, Z. Feng, C. Li, S. Maurer, U. Muller and F. S. Xiao, *J. Am. Chem. Soc.*, 2014, **136**, 4019–4025.
40 Y. Jin, Q. Sun, G. Qi, C. Yang, J. Xu, F. Chen, X. Meng, F. Deng and F. S. Xiao, *Angew. Chem., Int. Ed.*, 2013, **52**, 1–5.
41 T. H. Ngo, D. L. Tran, H. M. Do, V. H. Tran, V. H. le and X. P. Nguyen, *Adv. Nat. Sci.: Nanosci. Nanotechnol.*, 2010, **1**, 1–7.
42 J. Lu, S. Yang, K. M. Ng, C. H. Su, C. S. Yeh, Y. N. Wu and D. B. Shieh, *Nanotechnology*, 2006, **17**, 5812–5820.
43 P. Siemion, J. Kapusniak and J. J. Kozioł, *Carbohydr. Polym.*, 2005, **62**, 182–186.
44 C. A. Dyke and J. M. Tour, *J. Am. Chem. Soc.*, 2003, **125**, 1156–1157.
45 S. L. Y. Tang, R. L. Smith and M. Poliakoff, *Green Chem.*, 2005, **7**, 761–762.
46 W. Wardencki, J. Curyo and J. Namieœnik, *Pol. J. Environ. Stud.*, 2005, **14**, 389–395.
47 R. S. Varma, *Green Chem.*, 1999, **1**, 43–55.
48 V. Polshettiwar and R. S. Varma, *Green Chem.*, 2010, **12**, 743–754.
49 S. Ni, X. Wang, G. Zhou, F. Yang, J. Wang, Q. Wang and D. He, *Mater. Lett.*, 2009, **63**, 2701–2703.
50 M. Ma, Y. Zhang, W. Yu, H. Shen, H. Zhang and N. Gu, *Colloids Surf., A*, 2003, **212**, 219–226.
51 M. Khairya and M. E. Gouda, *J. Adv. Res.*, 2015, **6**, 555–562.
52 S. H. Hosseini and A. Asadnia, *J. Nanomater.*, 2012, **2012**, 1–6.
53 J. Li, H. Yuan, G. Li, Y. Liu and J. Leng, *J. Magn. Magn. Mater.*, 2010, **322**, 3396–3400.
54 R. M. Khafagy, *J. Alloys Compd.*, 2011, **509**, 9849–9857.
55 H. Yan, J. Zhang, C. You, Z. Song, B. Yu and Y. Shen, *Mater. Chem. Phys.*, 2009, **113**, 46–52.
56 R. W. Chantrell, N. S. Walmsley, J. Gore and M. Maylin, *J. Magn. Magn. Mater.*, 1999, **196–197**, 118–119.
57 W. Zhang, F. Shen and R. Hong, *Particuology*, 2011, **9**, 179–186.
58 W. Lu, Y. Shen, A. Xie and W. Zhang, *J. Magn. Magn. Mater.*, 2010, **322**, 1828–1833.
59 L. I. Cabrera, l. Somoza, J. F. Marco, C. J. Serna and M. P. Morales, *J. Nanopart. Res.*, 2012, **14**, 873–887.
60 Y. L. F. Musico, C. M. Santos, M. L. P. Dalida and D. F. Rodrigues, *J. Mater. Chem. A*, 2013, **1**, 3789–3796.
61 X. Wang, W. Liu, J. Tian, Z. Zhao, P. Hao, X. Kang, Y. Sang and H. Liu, *J. Mater. Chem. A*, 2014, **2**, 2599–2608.
62 S. T. Akar, D. Yilmazer, S. Celik, Y. Y. Balk and T. Akar, *Chem. Eng. J.*, 2015, **259**, 286–292.
63 H. Alijani, Z. Shariatinia and A. Aroujalian Mashhadi, *Chem. Eng. J.*, 2015, **281**, 468–481.
64 P. Sampranpiboon, P. Charnkeitkong and X. Feng, *WSEAS Trans. Environ. Dev.*, 2014, **10**, 35–47.
65 Y. Liu, X. Chang, S. Wang, Y. Guo, B. Din and S. Meng, *Anal. Chim. Acta*, 2004, **519**, 173–179.